http://www.journalmt.com

Research on FSW Welds of Al-Alloy Modified by Laser Shock Peening Process

Henrieta Chochlíková (0000-0003-4938-129X)[1], Jozef Majerík (0000-0002-6577-1987)[1], Igor Barényi (0000-0002-9296-600X)[1], Matúš Gavalec (0009-0009-9510-3793)[1], Jana Escherová (0000-0002-4203-2495)[1], Milan Pecanac (0000-0002-8016-9986)[2], Dragan Rajnovic (0000-0002-5303-4402)[2], Sebastian Baloš (0000-0002-3828-8500)[2], Marcel Kohutiar (0000-0002-4710-5913)[1]
[1]Faculty of Special Technology, Alexander Dubcek University of Trencin, Trenčín, 911 06, Slovakia, E-mail: jozef.majerik@tnuni.sk
[2]Faculty of Technical Sciences, University of Novi Sad, Novi Sad, 21000, Serbia, E-mail: pecanac.milan@uns.ac.rs

The friction stir welding (FSW) method is classified as a so-called green or eco-friendly production technology in terms of its environmental impact. In the process of friction stir welding, there is no melting and the weld joint is formed by the movement of a rotating tool between the materials to be welded. The advantage of this technology is welding without the accompanying phenomena such as the release of harmful substances into the air, the emission of infrared, ultraviolet and visible radiation, and low energy consumption. In this work, friction stir welding tests of FSW and SR-FSW type were carried out, the butt welds themselves were performed on EN AW - 6060 sheets of 5 mm thickness. The surfaces of the specimens that met the weld quality visually were treated with laser shock peening (LSP), which is based on a pulsed effect. In the process of experiments, the authors investigated the weld quality at different speeds and tool rotation visually, then the welds were subjected to microscopic analysis, microhardness analysis and nanohardness analysis.

Keywords: Friction Stir Welding FSW, Laser Shock Peening LSP, Aluminium alloy, Mechanical properties, Microstructural analysis

1 Introduction

Friction stir welding (FSW) was originally used exclusively for welding aluminum alloys and was invented and first used at The Welding Institute of the United Kingdom in 1991as a solid state welding technique [1, 2]. The basic principle of FSW is: A nonconsumable, geometrically specially designed rotating tool consisting of tool pin and tool shoulder is inserted into the edges of welded material sheets and the tool is guided along the plane of the future weld (see in Fig. 1). Figure 1 presents a schematic of the tool guidance in the workpiece during the FSW process [3].

The type of aluminum alloy EN AW-6060 is extrusion alloy which is widely used and suitable for applications where no need of special strength properties is. The material allows very good surface quality of the manufactured parts which is suitable for coating operations. A common field of application are automotive, architecture, home accessories and food industry.

The tool provides three basic functions, which are heating of the material, movement through the material to create the weld joint and holding of the hot metal beneath the shoulder of the tool. Friction which is created between the tool pin and tool shoulder generating the heat and a strong plastic deformation takes effect. Around the tool pin is localized heat, which softens the material and in the combination with tool rotational and translational movement leads to material flow, from the front side of the pin to its back side, which fills the space behind the tool as it moves forward. The flow of the metal is restricted by the tool shoulder to the level which is approximately at same height as the initial height of the workpiece [4]. After the FSW process, the four different material regions can be identified: Base Metal (BM), Heat Affected Zone (HAZ), Thermo-Mechanically Affected Zone (TMAZ) and Nugget Zone (NZ) [5, 12].

If the conditions set by a properly executed FSW process are met, a high-quality non-melting weld joint will be created. Each specific geometry of the tool has properties affecting the movement of the material around the tool pin and a characteristic rate of deformation, stress and heat gradients [6]. The microstructure of resulting Nugget zone is not homogeneous and reflects the different thermomechanical histories. The main benefit of FSW as a solid-state welding technique is that the material structure is fully recrystallized, equiaxed and the fine grain microstructure is created by the intense plastic deformation and elevated temperature in the spite of local microstructural inhomogeneity [7, 24].
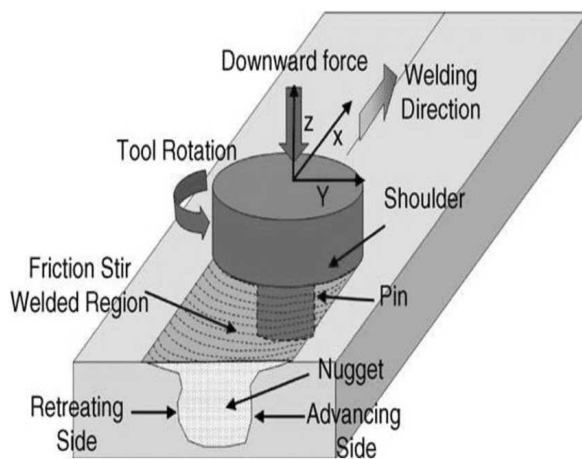
Fig. 1 *An overall view of principle of friction stir welding technological process [3]*

Mentioned fine grain microstructure is characterized by great mechanical and fatigue properties, enhanced formability and superplasticity [4].

Increasing of the rotation rate or decreasing of tool movement speed decrease the mechanical properties of the 2219Al-T651 FSW joints as was reported by Babu et al. [8]. While the increasing of the movement speed of the 2219Al-T6 FSW joints can increase the tensile strength and it is weakly dependent on the tool rotation rate, these conclusions were publicated by Zhang et al. [9]. Ren et al. [10] and Feng et al. [11] in their publications reported similar results and that the rotation speed was independent of the movement speed in 6061Al-T651 under the effect of increased tensile strength. That are the reasons why is the optimizing of FSW parameters so important for creating a high quality FSW joints. Mentioned parameters are different for every specific material.

During the FSW process can be avoided of the many problems which are observed by the traditional fusion welding methods. These problems are associated with the change of material state (change of volumetric and gas solubility) [14]. Traditional rotary friction welding (RFW) process is limited by the size of welding parts which are rotated and pushed against each other to a RFW joint formation [15-17], this problematic is by the FSW process eliminated. In the contrast of many other welding methods can FSW process reduce the residual stresses which are formed during the welding process and has a great application perspective in aluminum alloy [18], magnesium alloy [19], and other products [20-22]. The authors [23, 25] describe the FSW technology, where they investigated the influence of various parameters, including tool shapes, on the quality of the weld, and at the same time, the authors created a mathematical model of the overall quality of the obtained welds.

2 Experimental details, results & discussion

The first experiment was carried out with tool number one (see in Fig. 2), which removes some of the limitations of the FSW process, such as the necessity of using a backing plate or the presence of a keyhole at the end of the weld. The tool has an upper and lower arm that replaces the backing plate and helps in the creation of co-cuts. Welding process with the special geometry of the tool is called self-response friction stir welding (SR-FSW) [13].

The tool material chosen was tool steel produced by powder metallurgy heat treatment according to the attached Figure 3, the chemical composition of the tool material was verified by spectral analysis, the values are shown in Table 1. and the hardness of the tool was HV_{10} 458. Spectral analysis was performed on a SPECTROMAXx optical emission spectrometer, hardness measurement on a QATM Qness 250 CS evo hardness tester.

Tab. 1 *Chemical composition bobbin tool IC CH-11 [%]*

C	Si	Mn	P	S	Cr	Mo	Ni	Cu	V
0.37	0.79	0.36	0.02	0.005	4.96	1.2	0.19	0.164	0.34
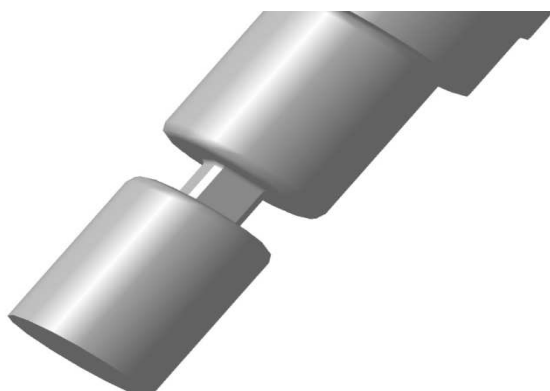
Fig. 2 *A view of the 3D display of so called Bobbin Tool (BT-FSW)*
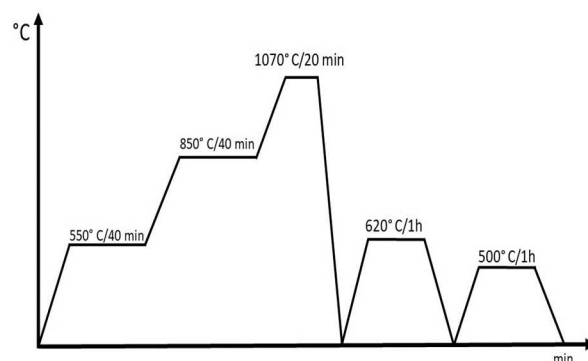
Fig. 3 *Overall view of the Heat Treatment mode of the tool called Bobbin Tool*

The material chosen for friction stir welding was precipitation hardenable aluminium alloy EN AW - 6060, blanks dimensions P5 50x480mm. Due to the combination of properties such as good hot formability and good hardened strength, this alloy is used for the production of various profiles. Corrosion resistance is good under normal atmospheric conditions. The weldability of the material is well weldable by common aluminium welding processes, especially MIG and TIG. During welding, there is a reduction in strength in the pre-transition zone, which can be corrected by appropriate heat treatment (dissolution annealing and hardening). EN AW-6060 T6 alloy is well machinable. The chemical composition of the above Al-alloy was measured on a SPECTROMAXx optical emission spectrometer, the values are recorded in Table 2.

Tab. 2 *Chemical composition EN AW – 6060/T66 (in wt. %)*

Si	Fe	Cu	Mn	Mg	Cr	Zn	Ti
0.532	0.205	0.043	0.055	0.425	0.013	0.026	0.016

The hardness of the above Al-alloy was measured on a QATM Qness 250 CS evo hardness tester and the micro-hardness on a QATM Qness 10 CHD MASTER+ micro-hardness tester. Hardness 85 HV 1, microhardness 85 HV 0.5.

Welding by FSW method was carried out on DM FP3-50 machine, during welding the working temperature was measured and the value was 200°C. Welding parameters feed rate, speed, distance "*h*" of the upper tool arm from the bottom surface can be seen in Table 3.

Tab. 3 *Parameters of welds performed by the SR-FSW method*

| Weld No.	Feed rate [mm.min⁻¹]	Speed [min⁻¹]	Distance H [mm]	Result
1	160	1440	4.8	Visually 1/5 of the weld length is Ok, Tool deformation in the middle of the path
2	200	1440	4.8	Poor quality weld after visual inspection
3	200	1440	5	Tool broken
4	100	1440	4.8	Poor quality weld after visual inspection
5	50	1440	4.8	Poor quality weld after visual inspection
6	50	1440	5	Poor quality weld after visual inspection
7	50	2000	5	Tool broken

An example of welds No. 2, 3, 4, and No. 6 is shown in Fig. 4
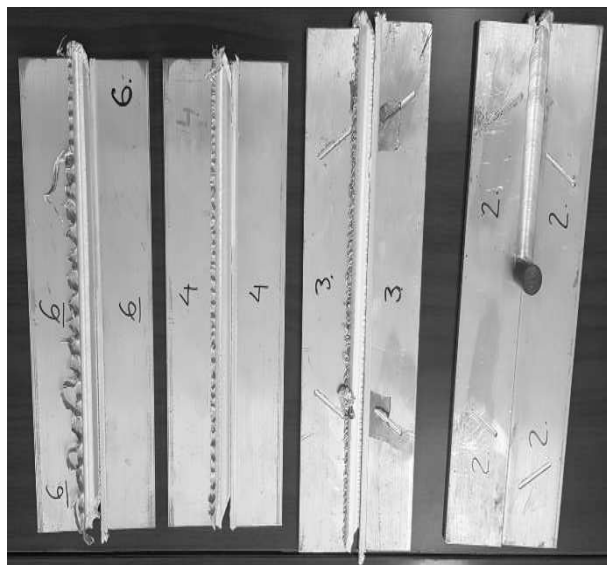
**Fig. 4** *A visual example of welds made by the method SR - FSW*

Despite the fact that the welds did not correspond to the specified quality after visual inspection, the welds were subjected to microscopic analysis by laser scanning confocal microscopy (LSCM)- brand Olympus LEXT OLS5100 3D Measuring Laser Microscope.

The macrostructures of the weld obtained from sample No. 1 at three different cross section cuts are shown in Fig. 5. The macrostructure in Fig. 5a was obtained 15 mm from the edge of the weld. The welded surfaces are only partially joined, unfilled voids are visible in the macrostructure. The macrostructure in the middle (Fig. 5b) was obtained at about 40 mm from the edge. The welded surfaces are properly mixed in the bottom part, which was supported by the lower tool arm. The upper part also contains voids. The macrostructure obtained at appx. 60 mm from the weld edge is shown in figure 5c. The faces are mixed most properly throughout the thickness in this case, but the small void is observed on the right side. The voids presence is caused by insufficient temperature in the weld area.
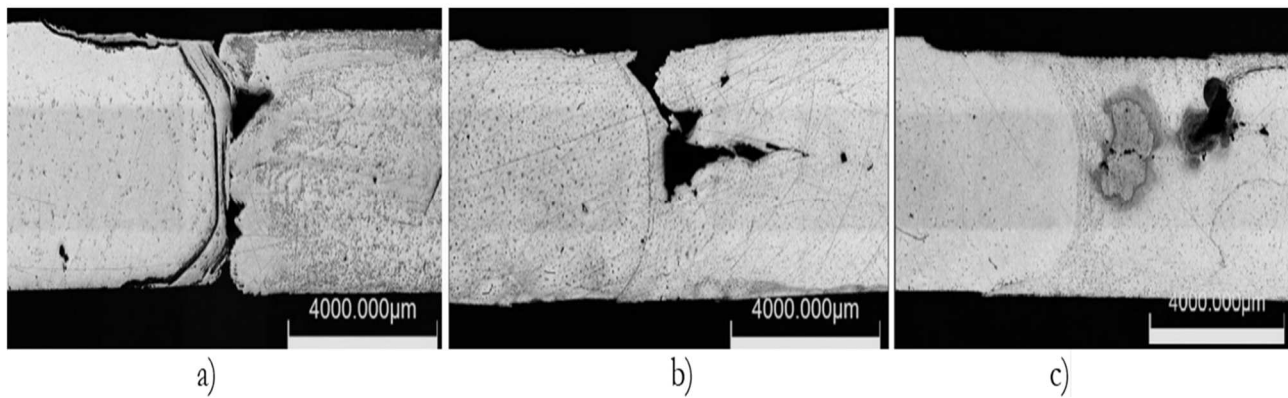
Fig. 5 *Macrostructure of weld on specimen 1 in three cross sections*

Also, the microhardness was measured on the QATM Qness 10 CHD MASTER+ microhardness tester on specimens 1 to 6 (according to Table 3). It is evident that there is a decrease in hardness in the middle of the weld where the two surfaces are connected by the FSW method, as is shown in Fig. 6. The spacing between the points in the the row is 0,5 mm and the row spacing is 1,5 mm.
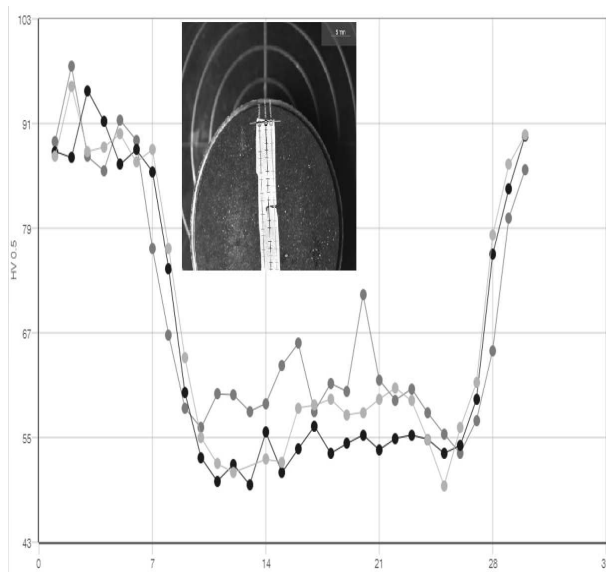

Fig. 6 *Microhardness coourse acrooss FSW weld of EN AW 6060 T66*

The second experiment was carried out using the FSW method with tool No. 2 (see in Fig. 7) made of H11 material, the shape of the tool is shown in Fig. 9. The material welded was EN AW 6060 T4, hardness 45 HV 1, microhardness 45 HV 0.5, the chemical composition was similar to that shown in Table 2. Welding parameters: feed rate = 160 mm.min^{-1}, speed = 1400 min^{-1}.

Since welding results in a reduction in strength in the transition zone, which can lead to a reduction in corrosion resistance and fatigue resistance. Our intention was to modify the surface by laser shock peening (LSP) in order to investigate or improve the weld surface. The specimens were immersed in distilled water, the distance between the water surface and the specimen surface was approximately 2 mm. LSP is based on the pulsed effect of the NdYAG laser, which, when focused on the surface of the sample, causes shock waves to propagate on the sur-face of the material.
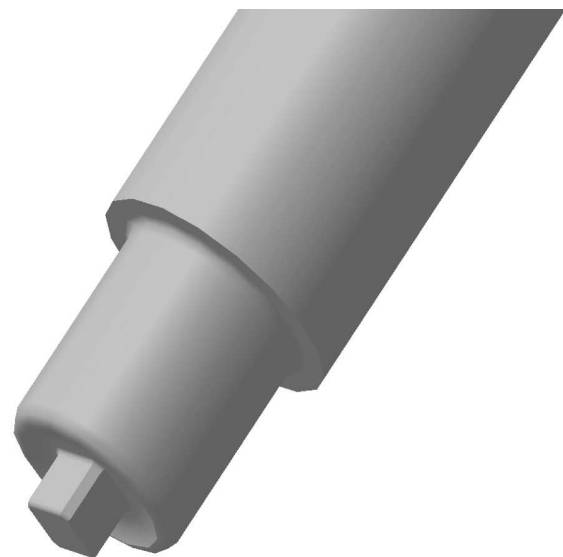
Fig. 7 *Example of the tool geometry used in the experiment No. 2*

These shock waves cause microstructural modifications in the material that induce residual compressive stresses. The pulsed laser effect was applied to both sides of the samples. Five welds were realized (see in Fig. 8), where the laser effect was applied on four of them at different parameters.

Table 4 shows the application parameters of the pulsed laser. Subsequently, the surface texture of the specimens was observed by evaluating the surface roughness, but no significant variations were observed in the comparison of the weld without and with the application of laser blasting.
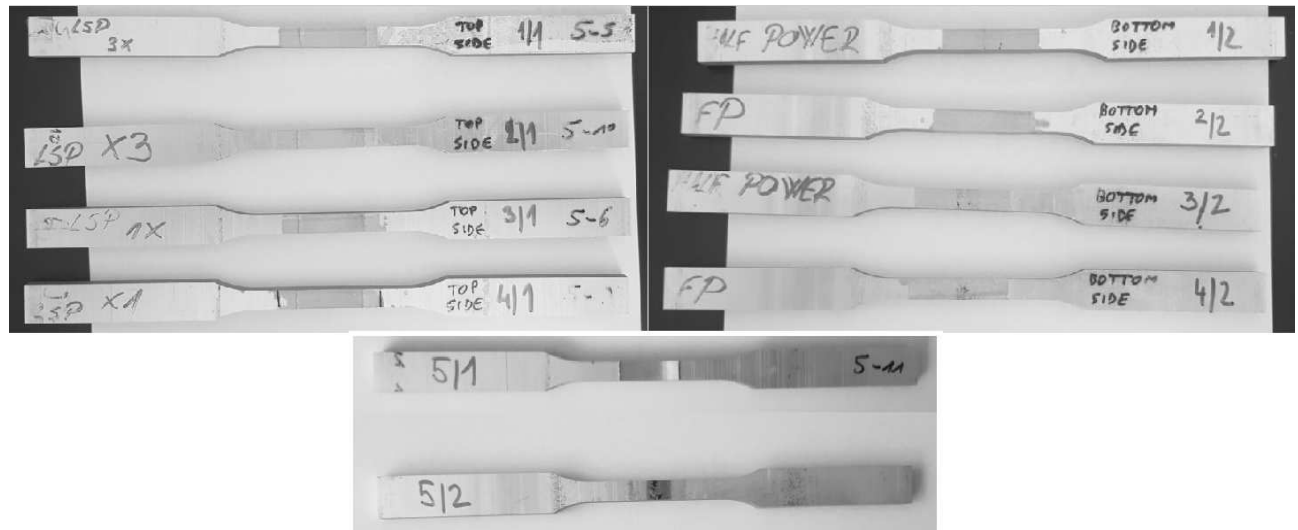
Fig. 8 *An overall view of the labelling of the test samples in the experiment No. 2*

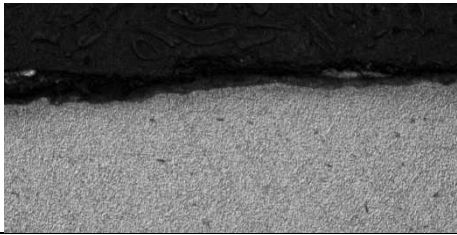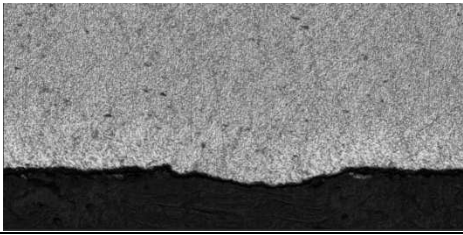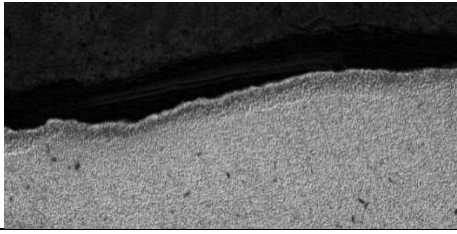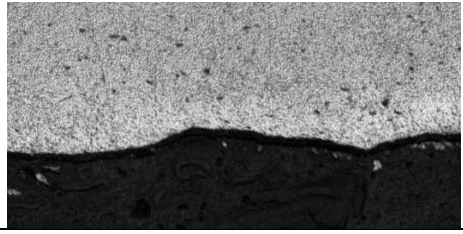**Tab. 4** *Parameters of LSP treatment used for individual samples*
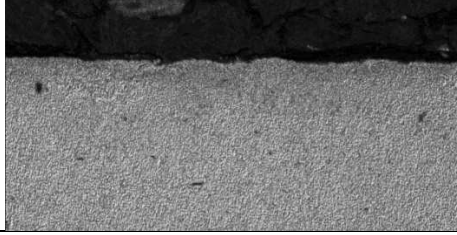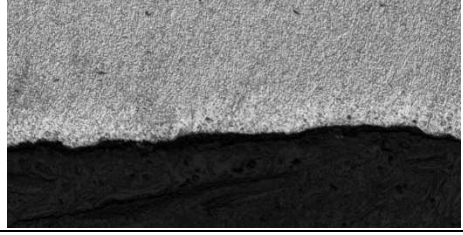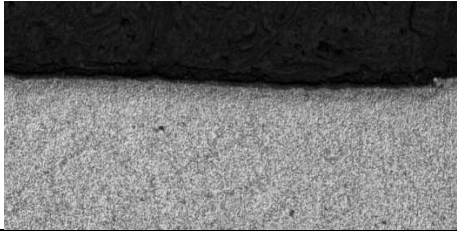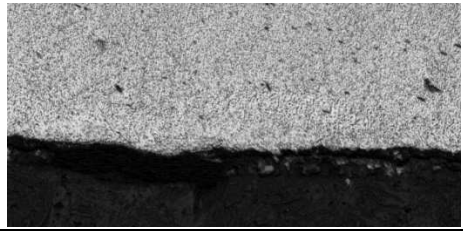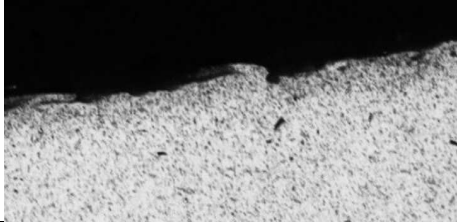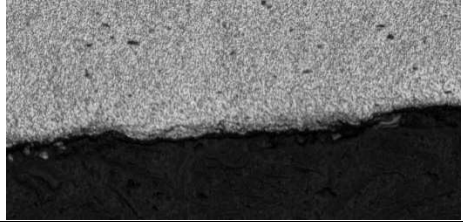
| Sample	Power	Number of laser passes (LSP)
1	HALF – 0.25 J	3
2	FULL – 0.5 J	3
3	HALF – 0.25 J	1
4	FULL – 0.5 J	1
5	untreated sample	

The welds were used to create samples for studying the microstructure of the surface layers, which were observed by laser scanning confocal microscope (LSKM)- Olympus LEXT OLS5100 3D. The scanning was performed with a 10 objective lens, zoom 1. Laser hardening was performed on both sides. Table 5 shows the images of the upper and lower edges.

The microstructures of observed specimens are very fine due to high deformation applied during FSW process. For the same reason, polygonal grains typical for this alloy in as-delivered state are not visible. LSP is carried out by immersing the sample in water, so the phase changes in the surface layers are not very pronounced. Regularly scattered Mg_2Si particles are observed in the structure. Under the influence of the heat supplied by the laser, uncontrolled dissolution annealing occurs in the subsurface layers. This results in a decrease in hardness, also confirmed by nanoindentation measurements. This affected layer is not optically distinct and poorly observable by light microscopy in a cases of half laser power and and one laser pass.

Next step were microhardness and nanohardness measurements. Nanohardness was measured on a HYSITRON Triboindenter TI 950 Nanoindenter. Microhardness was measured using the Vickers method with a load of 0.5 kg for $t = 10$ s. The course of microhardness is shown graphically in a series of graphs (see in Figures 9 to 13). Each graph is separate for a unique sample. On the X-axis, the points, 9 in number, are recorded, which were made by puncture, the distance between which was 0.5 mm. The number of bars is 6 evenly spaced as follows: marginal 1 and 6, central 3 and 4, and the other two are spaced 4.5 to the left and right of the center of the weld. In all cases (as can be seen in Fig. 9 - 13), the highest microhardness values are present in the middle of the welds, where the nugget area is present. This area is characterized with higher ration of plastic deformation causing thermo-mechanical treatment. Towards the edges of the weld, where the HAZ is located without the influence of thermomechanical strengthening, the hardness decreases.

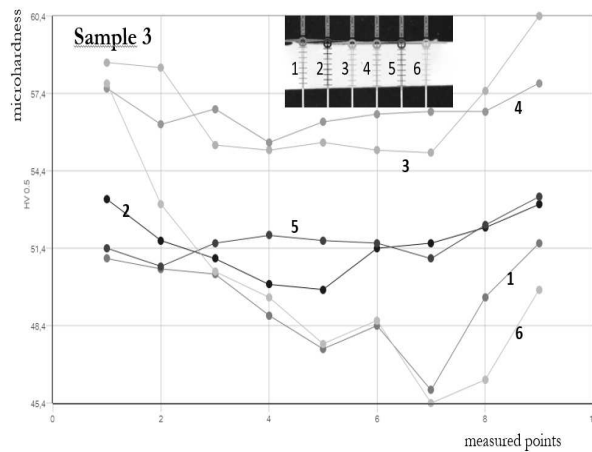**Tab. 5** *Microstructure of surface layers after the application of LSP*

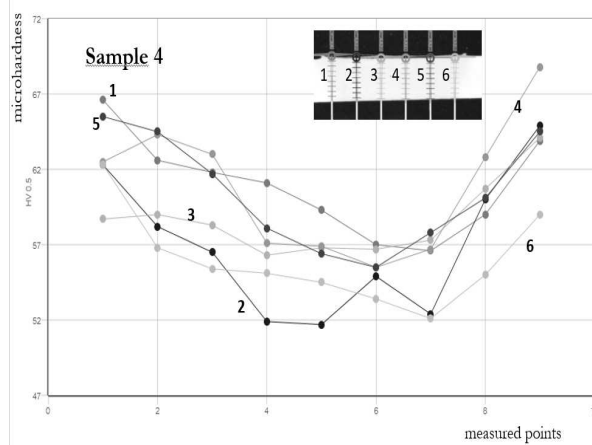| Sample		Top Edge	Bottom Edge
1	LSP 3x, half power		
2	LSP 3x, full power		
3	LSP 1x, half power		
4	LSP 1x, full power		
5	No LSP		
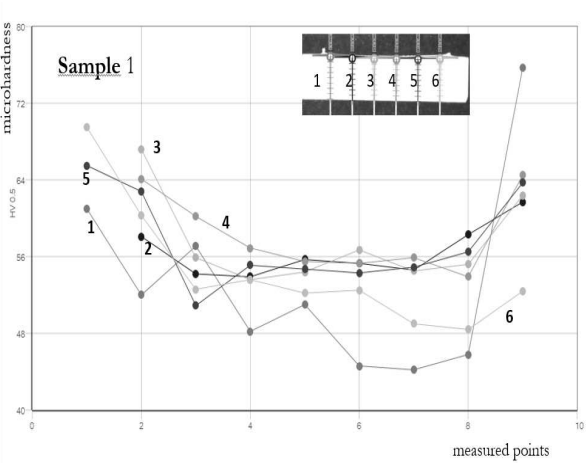
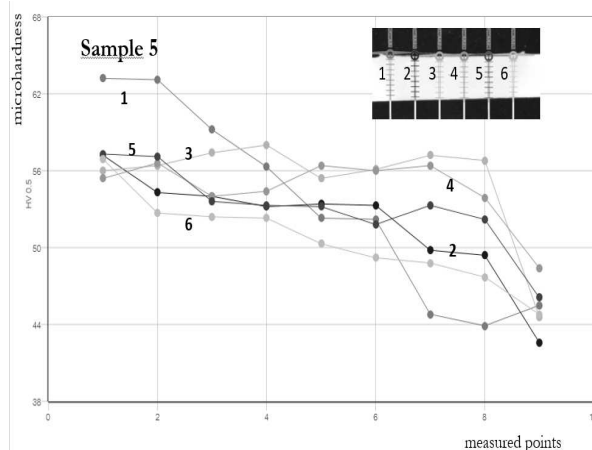**Fig. 9** *Microhardness course on sample 1 – FSW-LSP 3x at half*
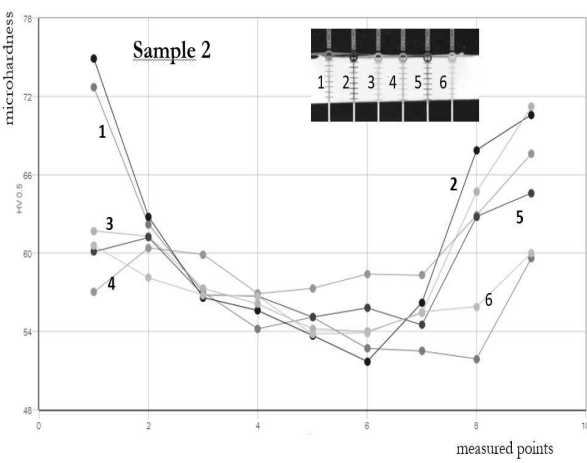
Fig. 10 *Microhardness course on sample 2 – FSW-LSP 3x at full power*

**Fig. 11** *Microhardness course on sample 3– FSW-LSP 1x at half power*

Fig. 12 *Microhardness course on sample 4– FSW-LSP 1x at full power*

Fig. 13 *Microhardness course on sample 5 – FSW- without LSP treatment*

The nanohardness (Fig. 14) was measured for individual samples from 1 to 56 to confirm hardness changes of subsurfaced areas caused by LSP treatment. The nano hardness course has the same typical shape in cases where full power laser was used (sample

1,2) or laser has three passes (sample 4). The nanohardness is lower just below the surface, then increases to the local maximum in a depth of 50-70 μm and finally decreases to the value of the base material. The maximal peak is most shifted to the right in a case of three passes with full laser power (Sample 2). Sample 3 (one laser pass with half power) shows almost the same hardness profile as non-treated weld ant thus does not exhibit the influence by the LSP.
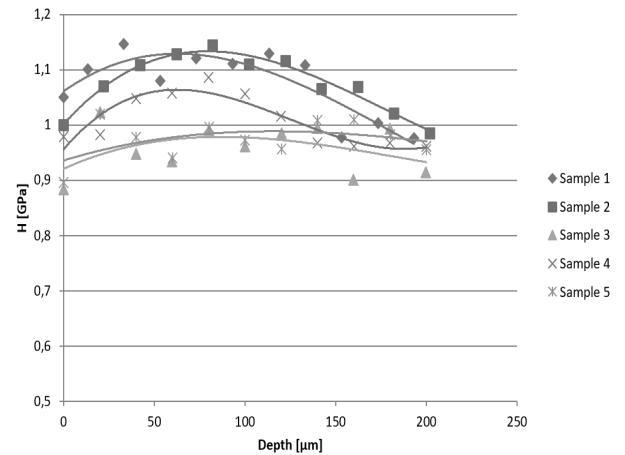
Fig. 14 *Nanohardness course of samples treated by difftent FSW-LSP parameters*

3 Conclusion

The following observations emerged from the range of experiments carried out by the team of authors, which are formulated in the following conclusions. It can be said that microhardness courses across weld areas corresponds with typical FSW weld areas. Microhardness is higher in zones with TMT effect in the middle of the weld and decreases towards the weld edge. LSP treating was evaluated by microstructure observation and nanohardness testing of sub surface areas of individual samples. The affected zone is partially visible only in a case of three passes of the laser with full power. Also nanohardness course shows the affection only in cases with full laser power or three passes. The case of LSP with one pass and half laser power do not show more significant change in compare to LSP non treated material. The achieved results also open space for further research by the authors of the international team. The intention is to continue experiment 1, but to set the parameters in such a way that a higher temperature is achieved.

References

[1] THOMAS, W. M., NICHOLAS, E. D., NEEDHAM, J. C., MURCH, M. G., TEMPLESMITH P., DAWES C. J. 1991. G. B. *Patent* 9125978.8.

[2] DAWES, C., THOMAS, W. 1995. TWI Bull. p 124.

[3] CHANDRAN, R., SENTHIL KUMAR, V.S. 2015. Submerged Friction Stir Welding and Processing: Insights of Other Researchers. *International Journal of Applied Engineering Research.* 10. 6530-6536.

[4] MISHRA, R. S., MAHONEY, M. W. 2007. *Friction stir welding and processing.* ISBN-13: 978-0-87170-840-3.

[5] K. ELANGOVAN; V. BALASUBRAMANIAN. 2008. Influences of tool pin profile and tool shoulder diameter on the formation of friction stir processing zone in AA6061 aluminium alloy. *Mater. Des.* 29 (2008) 362–373.

[6] LIU, G., MURR, L. E.; NIOU, C. S., MC-CLURE, J. C., VEGA, F. R. 1997. Microstructural aspects of the friction-stir welding of 6061-T6 aluminum. *Scr. Mater.* Vol 37. p 355.

[7] JATA, K. V., SEMIATIN S. L. 2000. Continuous dynamic recrystallization during friction stir welding of high strength aluminum alloys. *Scr. Mater.* Vol 43. p 743.

[8] BABU, S., ELANGOVAN, K., BALASUBRAMANIAN, V., BALASUBRAMANIAN, M. 2009. Optimizing friction stir welding parameters to maximize tensile strength of AA2219 aluminum alloy joints. *Met. Mater. Int.* 15. 321–330.

[9] ZHANG, Z., XIAO, B.L., MA, Z.Y. 2012. Effect of welding parameters on microstructure and mechanical properties of friction stir welded 2219Al-T6 joints. *J. Mater. Sci.* 47. 4075–4086.

[10] REN, S. R., MA, Z.Y., CHEN, L.Q. 2007. Effect of welding parameters on tensile properties and fracture behavior of friction stir welded Al–Mg–Si alloy. *Scr. Mater.* 56. 69–72.

[11] FENG, A., CHEN, D., MA, Z. 2010. Microstructure and Cyclic Deformation Behavior of a Friction-Stir-Welded 7075 Al Alloy. *Metall Mater Trans A* 41, 957–971.

[12] CAMPANELLI, S. L., CASALINO, G., CASAVOLA, C., MORAMARCO, V. 2013. Analysis and Comparison of Friction Stir Welding and Laser Assisted Friction Stir Welding of Aluminum Alloy. In: *Materials* 2013, 6, 5923-5941; doi:10.3390/ma6125923. ISSN 1996-1944

[13] TRUEBA, L., TORRES, M. A., JOHANNES, L. B., RYBICKI, D. 2017. Process optimization in the self-reacting friction stir welding of aluminum 6061-T6. In: *Int J Mater* from (2018) 11:559-570. DOI 10.1007/s12289-017-1365-4

[14] LOHWASSER, D., CHEN, Z. 2010. *Friction stir welding from basics to applications.* Woodhead Publishing Ltd. pp:15-20.

[15] CARY, H. B. 2005 *Modern welding technology.* Prentice Hall

[16] GAVALEC, M., BARÉNYI, I., CHOCHLIKOVA, H. 2022. Properties and microstructure of joints created by the method of rotary friction welding, *Zborník prednášok z 31. medzinárodnej konferencie metalurgie a materiálov METAL 2022,* Brno.

[17] GAVALEC, M., BARÉNYI, I., KRBAŤA, M., KOHUTIAR, M., BALOS, S., PECENAC, M. 2023. The Effect of Rotary Friction Welding Conditions on the Microstructure and Mechanical Properties of Ti6Al4V Titanium Alloy Welds. MDPI *Materials,* 2023, 16, 6492.

[18] GOMATHISANKAR, M., GANGATHARAN, M., PITCHIPOO, P. 2018. A Novel Optimization of Friction Stir Welding Process Parameters on Aluminum Alloy 6061-T6. *Mater. Today: Proceedings,* Vol. 5. p. 14397-14404.

[19] PAN, F.S., XU, A.L., DENG, D.A., et al. 2016. Effects of friction stir welding on microstructure and mechanical properties of magnesium alloy Mg-5Al-3Sn. *Mater. Des.* Vol. 110. p.266-274.

[20] CHUMAEVSKII, A., AMIROV, A., IVANOV, A., RUBTSOV, V., KOLUBAEV, E. 2023. Friction Stir Welding/Processing of Various Metals with Working Tools of Different Materials and Its Peculiarities for Titanium Alloys. *Metals* 13. 970.

[21] MAO, Y., KE, L., LIU F., et al. 2015. Effect of welding parameters on microstructure and mechanical properties of friction stir welded joints of 2060 aluminum lithium alloy. *Int J Adv Manuf Technol* 81, 1419–1431.

[22] XU, A. 2020. Properties of High-Speed Friction Stir Welded 6063-T6 Aluminum Alloy. *J. Phys.: Conf. Ser.* 1676.

[23] KAMMINANA, R., KAMBAGOWNI, V. S. 2022, Multi response optimization of friction stir welding of AA2050 using response surface methodology coupled with grey relational analysis and principal component analysis. *Manufacturing Technology*, Vol. 22, p. 156-167.

[24] KOSTUREK, R., ŚNIEŻEK, L., GRZELAK, K., TORZEWSKI, J. 2021, Study on the weldability of AA2519 armor grade aluminium alloy. *Manufacturing Technology*, Vol. 21, p. 818-823.

[25] KVASNOVÁ, P., NOVÁK, D., NOVÁK, V., ĎURIŠ, M. 2023, Computer Simulation of heating cycle of aluminium alloys using friction stir welding technology. *Manufacturing Technology*, Vol. 23, p. 47-52.